

## 2-2-4 Application of the Magnetospheric Model for Numerical Forecast – Validation Using the Cross Polar Cap Potential –

**KUNITAKE Manabu, WATARI Shinichi, SHINAGAWA Hiroyuki, SHIMAZU Hironori, NAGATSUMA Tsutomu, HORI Tomoaki, FUJITA Shigeru, and TANAKA Takashi**

National Institute of Information and Communications Technology (NICT) has been running the real-time magnetohydrodynamic (MHD) simulation of the magnetosphere-ionosphere (M-I) coupling system[1]–[4]. The 2-D ionospheric electric potential distribution can be reproduced from the real-time run of the magnetosphere simulation. We extracted parameters, such as, the locations of potential MAX and MIN and the magnitude of potential MAX (Potmax) and the absolute value of potential MIN (IPotmin|), and the cross polar cap potential (CPCP; the difference between maximal and minimal values of the potential = Potmax – Potmin) from the 2-D ionospheric potential distribution, then made statistical analyses about the dependence of these parameters on the solar wind. Further, the simulation results were compared with the results of Weimer 2001 model [5] on the same solar wind condition. The statistical analyses and comparison analyses revealed the following: (1) the CPCP value resulting from simulation is almost always greater than that yielded by the Weimer 2001 model, (2) the magnitude relation between Potmax and absolute Potmin (|Potmin|) is Potmax > |Potmin| resulting from simulation and Potmax < |Potmin| from the Weimer 2001 model when the Y component (“By”) of the interplanetary magnetic field (IMF) is negative, and (3) magnetic local time (MLT) corresponding to the locations of maximal and minimal potentials was on the nightside more with the Weimer 2001 model than with simulation. Based on these results, we have presumed that the day-to-night gradient in the ionospheric conductance in our simulation would not be as steep as that in the actual ionosphere.

### **Keywords**

MHD simulation, Polar cap potential, Solar wind dependence, Ionospheric conductance, Statistical analyses

### **1 Introduction**

NICT has regularly been running the magnetohydrodynamic (MHD) simulator of the magnetosphere-ionosphere coupling system in real time using ACE observational data as input for upstream boundary conditions[1]–[4]. ACE is an artificial satellite located at the L1 point (a point where gravity of the sun and

earth are in equilibrium) at a distance of about 220 earth radii (Re) from the earth toward the sun. The results obtained from running real-time simulation are accumulated on hard disk. Thus, running simulation for a prolonged period creates a database consisting of simulation results under a variety of actual solar wind conditions. Statistical analysis using the huge amount of calculation results saved in this

database is conducted to enable a systematic study of the characteristics (e.g., dependence on solar wind) of MHD simulations. Therefore, arranging these statistical results and giving due consideration to physics make it possible to better understand the characteristics and problems of these simulations.

From a validation point of view, it is vital to study whether the above-mentioned characteristics are consistent with those indicated by observations. An evaluation is conducted by comparing the results from an empirical model based on observations with the simulation calculation results to determine the extent to which the simulation can reproduce reality. As the next step in case that some discrepancy is found in this comparison, the reasons for such discrepancy are searched and the knowledge thus acquired is fed back for improving the simulation.

A validation study on the auroral electrojet current flowing in the polar region is an example of past studies involving statistical analyses using this database[6]. The auroral electrojet current (expressed by the AE index) has been validated in this simulation for fairly good reproducibility through a comparative analysis of the AE index derived from this simulation with that provided by observations[4][6][7].

This paper deals with the electric field. One output from this simulation is a two-dimensional distribution of the electric potential of the polar ionosphere. Physical parameters extractable from this distribution are the maximal and minimal values of the potential, the latitudes and magnetic local times (MLT) to which the maximal and minimal values correspond, and so on. Moreover, the cross-polar cap potential (CPCP value) can also be determined. The CPCP value — a scalar quantity of the maximal value minus the minimal value of the potential — is a quantity frequently used in studies on the solar wind magnetosphere coupling for providing an overall picture of the electric potential applied by the magnetosphere to the ionosphere[8]. This paper reports the results of a systematic study conducted on the dependence on solar wind as

pertaining to the parameters above. We mindfully studied this dependence not only on simple physical quantities such as solar wind velocity but also on such physical quantities likely related to potential distribution as the IMF clock angle and merging electric field (Emerg). Thus, this paper only describes the results considered essential. The period analyzed is from January 1 to May 10, 2006. This period corresponds to the minimal period of solar activity. The above-mentioned parameters were based on hourly averages for use.

The following explains some coordinates and variables used in this report.

**GSM coordinates:** Defined as the X-axis as directed from the center of the earth toward the center of the sun, the Y-axis perpendicular to the plane comprised of the earth's dipole axis and said X-axis, and the Z-axis configuring a right-handed orthogonal system with said X- and Y-axes.

The IMF clock angle (theta) is derived from the following equations:

$$Byz = (By^2 + Bz^2)^{\frac{1}{2}} \quad (1)$$

$$\text{theta} = \text{Arccos}(Bz/Byz) \quad (2)$$

**By:** Y component of the magnetic field on the GSM coordinates

**Bz:** Z component of the magnetic field on the GSM coordinates

**Byz:** Magnetic field intensity on the YZ plane of the GSM coordinates

**Emerg** is derived from the following equation:

$$\text{Emerg} = V \times Byz \times \{\sin(\text{theta}/2)\}^2 \quad (3)$$

**V:** Solar wind velocity

By comparing the simulation to an empirical model based on observations, the simulation is evaluated for its reproducibility of actual situations. The Weimer 2001 model[5] is used as an empirical model and the results of

statistical and comparative analyses are reported. Two different types were used for comparative analysis. One covers both simulation and empirical model results, in order to study the dependence on solar wind as pertaining to a particular physical quantity, and the differences and similarities of regarding dependence on solar wind between both types. The other is intended for a particular physical quantity at the same clock time, in order to statistically study the direct correspondence relation between the simulation and empirical model results.

The discrepancy between the simulation and empirical model results as determined by such comparisons are considered for cause, the knowledge acquired in the consideration process is thus fed back, and proposals for improving this simulation are presented as a summary of this study.

## 2 Notes on statistical analysis of the database of simulation results

The dipole tilt angle (formed by the earth's rotational axis and the geomagnetic dipole axis) is fixed to  $0^\circ$ . In other words, this refers to the angle at which the rotational and dipole axes coincide. Since the rotational axis is set to be always perpendicular to the ecliptic plane, the ionospheric conductance distribution due to solar extreme ultraviolet radiation (solar EUV) is that under conditions of the spring and autumn equinoxes. The values on the GSM coordinates are thus used as inputs for ACE observational data on the interplanetary magnetic field (IMF). Note that using a value of 0 for the Bx component is inevitable for simulation, even if observational data does not provide a value of 0.

The input range is restricted in order to stably and continuously run the simulator in real time [4]. The upper limits in the following equations are used for the input range of simulation; the upper limit is continuously used in case an ACE solar wind observational value approaches or exceeds the upper limit. A simi-

lar condition also applies to the lower limit.

IMF By component:

$$-7.5 \text{ nT} < B_y < 7.5 \text{ nT} \quad (4)$$

IMF Bz component:

$$-13 \text{ nT} < B_z < 13 \text{ nT} \quad (5)$$

Solar wind density n:

$$3.3/\text{cc} < n < 10/\text{cc} \quad (6)$$

Solar wind velocity V:

$$124 \text{ km/s} < V < 899 \text{ km/s} \quad (7)$$

Solar wind temperature T:

$$112200 \text{ K} < T < 204000 \text{ K} \quad (8)$$

Thus, the dataset used for statistical analysis only picks up the periods of time that are correctly assignable with the ACE observational values (i.e., periods of time when ACE observational values fall within the set input range). The periods of time when ACE observational values exceed the input range are discarded. However, the periods when temperature exceeds the input range are not discarded, provided that the dependence on temperature is not analyzed, as very few periods of time fall within the input range.

During periods of time when the IMF Bz component is negative or in the southward direction, the polar ionospheric plasma convection in the potential distribution projected in the ionosphere is known to have two vortices — one each on the dawn and dusk sides (two cell convection). The vortices flow counterclockwise on the dawn side and clockwise on the dusk side (see Fig. 1). In contrast, the potential distribution is much more complex during periods of time when the IMF Bz component is positive. For example, in case of three or four vortices, extracting and interpreting the parameters become more difficult. Thus, it was decided to discard the periods of time for positive IMF Bz, so as to pick up only those periods for negative IMF Bz with two vortices expected to appear.

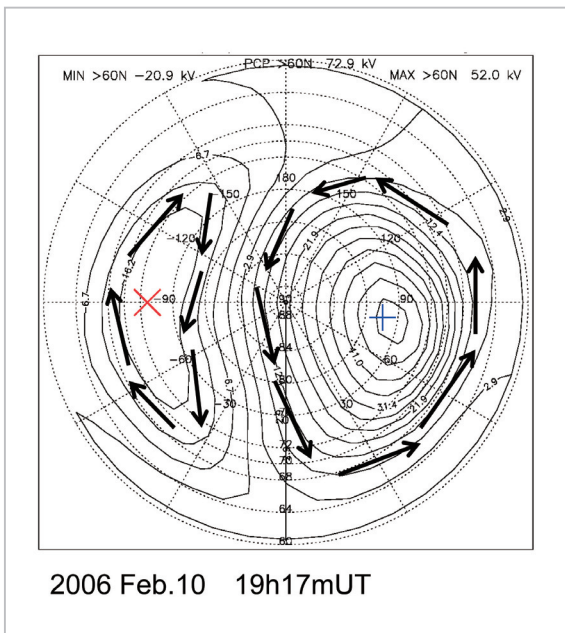


**Fig. 1** Example of potential distribution calculated from simulation

The contour lines represent electric field potentials. Blue “+” symbol denotes the position of maximal potential; red “X” symbol denotes that of minimal potential. Arrows indicate the convection directions of plasma in the ionosphere. Note that the lengths of arrows do not correspond to the magnitude of velocity.

### 3 Weimer 2001 model

The Weimer 2001 model was empirically derived based on solar wind observations by the IMP 8 and ISEE 3 satellites, and electric field observations by the DE2 satellite (in a low-altitude polar orbit). The inputs are solar wind velocity, solar wind density, IMF Byz (magnetic field intensity on the YZ plane of the GSM coordinates), IMF clock angle, dipole tilt angle, and AL index for polar disturbances. An available output is the two-dimensional distribution of the electric potential of the polar ionosphere.

In the comparative analyses conducted for this study, ACE observational data which were adopted as the boundary condition of the simulation were also provided as input for the Weimer 2001 model (at the clock time used for simulation), in order to obtain a two-dimensional potential distribution of the polar

ionosphere as output. To further match the conditions, the tilt angle (as one setting parameter) was fixed to 0, similarly to the simulation, in calculations using the Weimer 2001 model. The AL index used was the provisional AL index calculated by the World Data Center for Geomagnetism, Kyoto.

Note the following points:

The MHD simulation used the ACE observational data received in real time, while the Weimer 2001 model used calibrated Level 2 data as input (even though the clock time was the same). For a more rigorous comparison, the ACE observational data received in real time must be extracted and input into the Weimer 2001 model; however, the estimated significant amounts of time and labor required mandated the use of Level 2 data as input for the Weimer 2001 model.

## 4 Analysis results

### 4.1 Merging electric field (Emerg) dependence of the CPCP value

Figure 2 is plotted with simulated CPCP values on the Y-axis and Emerg on the X-axis. A linear least-square fitted curve is also superimposed based on the following equation:

$$\text{CPCPfit} = a + b \times \text{Emerg} \quad (9)$$

The correlation coefficient is high at 0.832. Intercept “a” is 45.470 and gradient “b” 26.226.

Figure 3 illustrates the results from a correlation analysis similar to the above by using the Weimer 2001 model. The correlation coefficient is high at 0.939. Intercept “a” is 32.574 and gradient “b” 20.267.

What is understood from these two diagrams are: (1) both show high correlation with Emerg and can be approximated with a linear function, and (2) the simulation results tend to show somewhat larger CPCP values than the Weimer 2001 model.

Figure 4 illustrates a direct comparison of CPCP values yielded by the simulation and Weimer 2001 model at the same clock time. The vertical axis represents the CPCP value

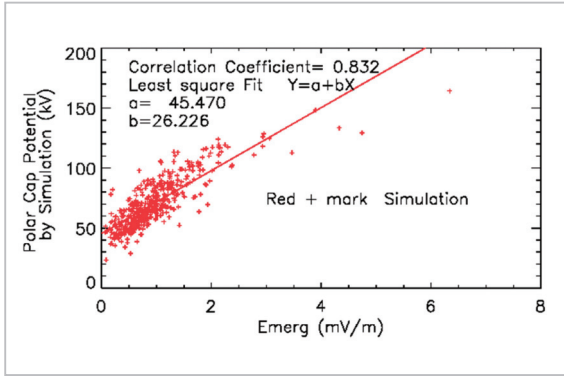


**Fig.2** Comparison of CPCP values resulting from simulation with merging electric field and the regression line

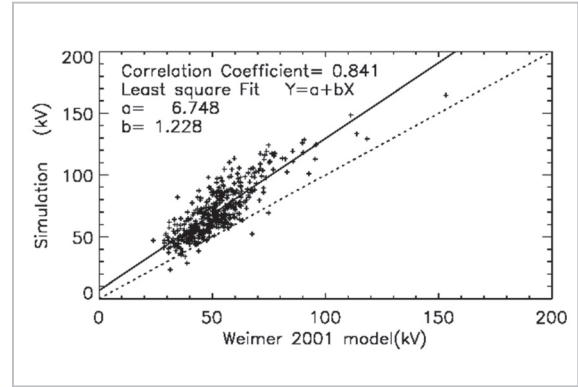


**Fig.4** Comparative diagram of CPCP value results from simulation and the Weimer 2001 model

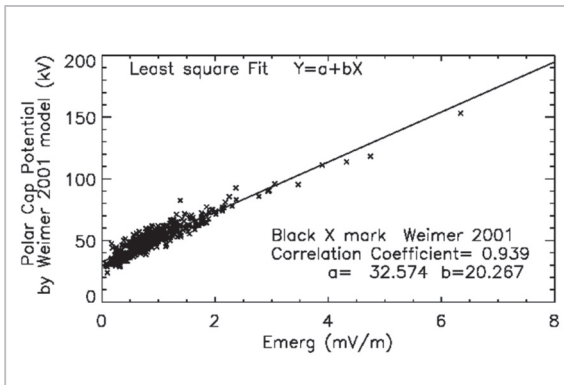


**Fig.3** Comparison of CPCP values resulting from the Weimer 2001 model with merging electric field and the regression line

from the simulation; the horizontal axis represents that from the Weimer 2001 model. In addition, a linear least-square fitted line by the following equation is superimposed using a solid line.

$$CPCP_{simfit} = a + b \times CPCP_{weimer} \quad (10)$$

The correlation coefficient is high at 0.841. Intercept “a” is 6.748 and gradient “b” 1.228. Note that the angled dotted line in the figure indicates the identical CPCP values assumed to result from both the simulation and Weimer 2001 model. Being easily recognizable, the CPCP values resulting from simulation are in most cases greater than those from the Weimer 2001 model. The CPCP values from simulation are found to be highly correlated with those from the Weimer 2001 model, and could

be derived from the linear equation.

#### 4.2 IMF clock angle dependence of magnitude relation between maximal value and absolute value of minimal value of potential

In case that ionospheric convection is a two-cell convection, the potential appears to reach its maximal value (Potmax) and minimal value (Potmin) at the center of vortices on the dawn and dusk sides, respectively, where Potmin is a negative value. We studied the magnitude relation between Potmax and absolute Potmin by calculating the difference between both and normalizing it with the CPCP value.

$$Ratediffpot = (Potmax - |Potmin|) / (Potmax + |Potmin|) \quad (11)$$

The following can be determined: Potmax and |Potmin| are about the same when Ratediffpot is near 0, Potmax is predominantly greater than |Potmin| when Ratediffpot is near 1, and Potmax is predominantly less than |Potmin| when Ratediffpot is near -1. Figure 5 (a) illustrates the simulation results with Ratediffpot on the vertical axis and the IMF clock angle on the horizontal axis. With a clock angle of about 90° or positive By, Potmax is somewhat less than |Potmin|. Conversely, with a clock angle of about 270° or negative By, Potmax is somewhat greater than |Potmin|. The same plotting

method was applied to the Weimer 2001 model (Fig. 5 (b)). In case of a clock angle from  $90^\circ$  to  $270^\circ$ , Potmax is usually less than |Potmin|. That is, with negative  $B_z$ , the potential appears to be  $\text{Potmax} < |\text{Potmin}|$  in most examples regardless of negative or positive  $B_y$ .

### 4.3 IMF clock angle dependence of MLT at locations corresponding to maximal and minimal values of potential

The locations of the maximal and minimal potential values correspond to the centers of vortices in ionospheric convection. Figures 6 (a) and (b) show diagrams with the clock angle on the

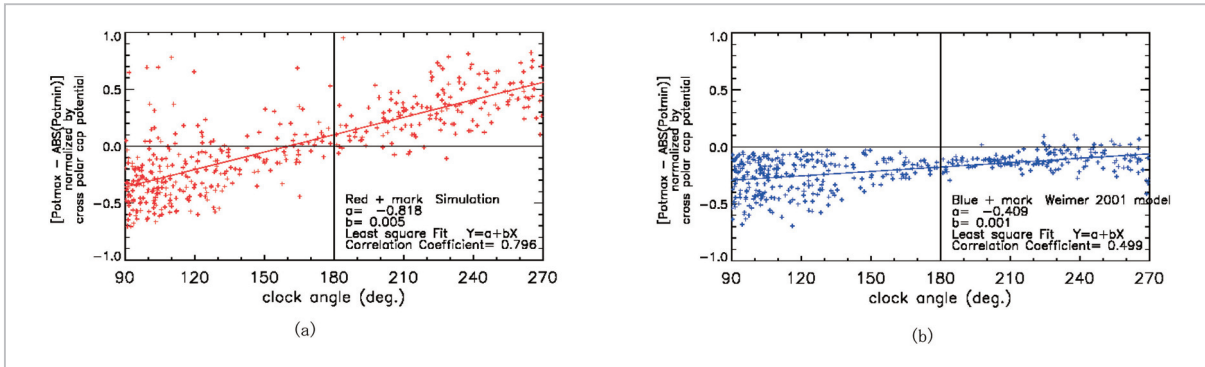


**Fig.5** IMF clock angle dependence of difference between the dawn and dusk sides of potential  
 (a): Simulation, (b): Weimer 2001 model

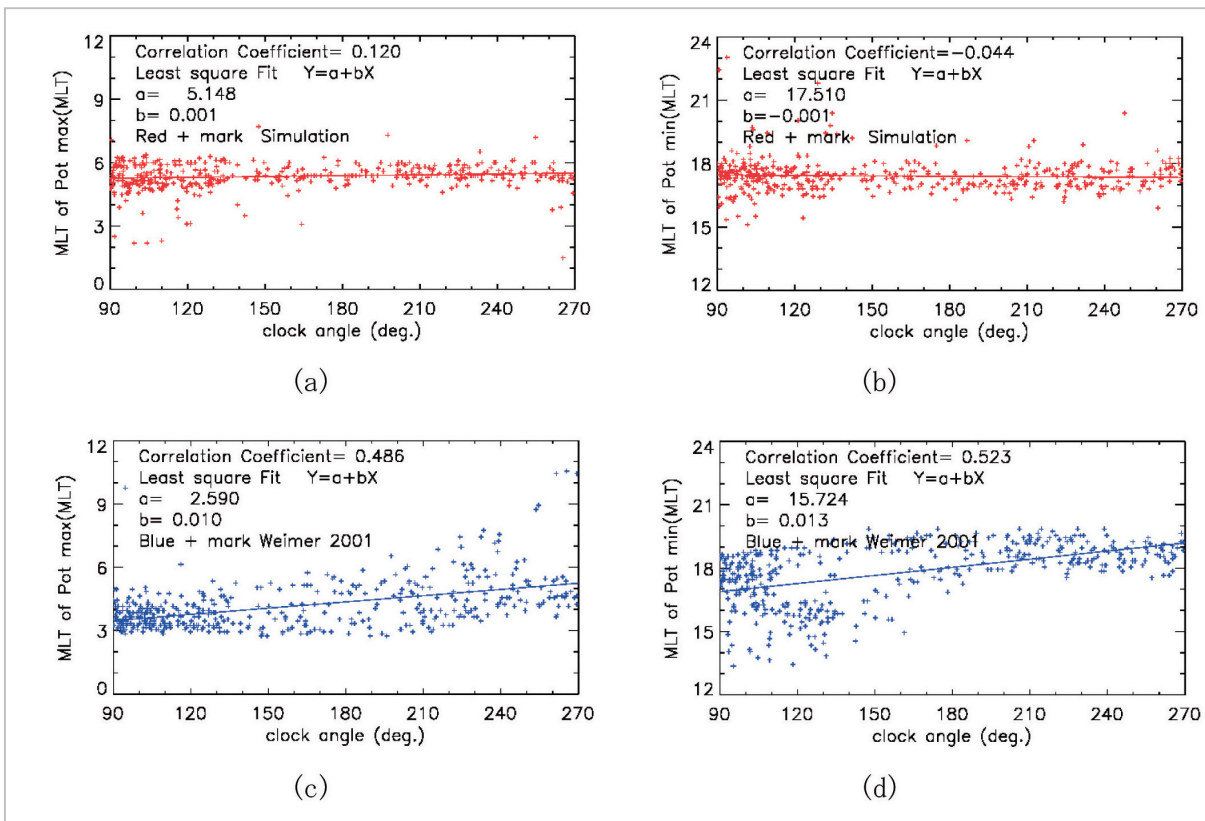


**Fig.6** Clock angle dependence of MLTs corresponding to locations of maximal and minimal potential values

- (a) MLT corresponding to the location of maximal potential value for simulation,
- (b) MLT corresponding to the location of minimal potential value for simulation,
- (c) MLT corresponding to the location of maximal potential value for the Weimer 2001 model, and
- (d) MLT corresponding to the location of minimal potential value for the Weimer 2001 model

X-axis, and MLTs corresponding to locations at the center of cells on the dawn side (maximal potential) and dusk side (minimal potential) on the Y-axis. Both MLTs corresponding to locations of the maximal and minimal potential values indicate no systematic change with respect to the clock angle. With some dispersion present, MLT corresponding to the maximal potential is about 5hMLT and that to the minimal potential about 17hMLT.

Figures 6 (c) and (d) show the clock angle dependence when the same plotting method was applied to the Weimer 2001 model. The results obtained from the Weimer 2001 model differ significantly from those from the simulation. The dispersion in MLT corresponding to the locations of maximal potential increases as the clock angle increases (or as  $B_y$  moves from positive toward negative). For example, at a clock angle of  $90^\circ$  with small dispersion, MLT is about 3hMLT to 4hMLT. The dispersion in MLT corresponding to the locations of minimal potential increases as the clock angle decreases (or as  $B_y$  moves from negative toward positive). At a clock angle of  $270^\circ$  with small dispersion, MLT is about 19hMLT.

A direct comparison was also made between the simulation results and Weimer 2001 model results at the same clock time. Figures 7 (a) and (b) show comparative diagrams of MLTs corresponding to the locations of maximal and minimal potentials, respectively. Note that the angled dotted line in each figure indicates MLT assumed to be identical as resulting from both the simulation and Weimer 2001 model. In Fig. 7 (a) where MLTs corresponding to the maximal potential are plotted, most plots are located in the top-left area of the dotted line. This means that MLTs corresponding to the maximal potential are in most cases distributed on the nightside in the Weimer 2001 model as compared to the simulation. In Fig. 7 (b) where MLTs corresponding to the minimal potential are plotted, a significant number of plots are located in the bottom-right area of the dotted line. This means that MLTs corresponding to the minimal potential are distributed on the nightside in a

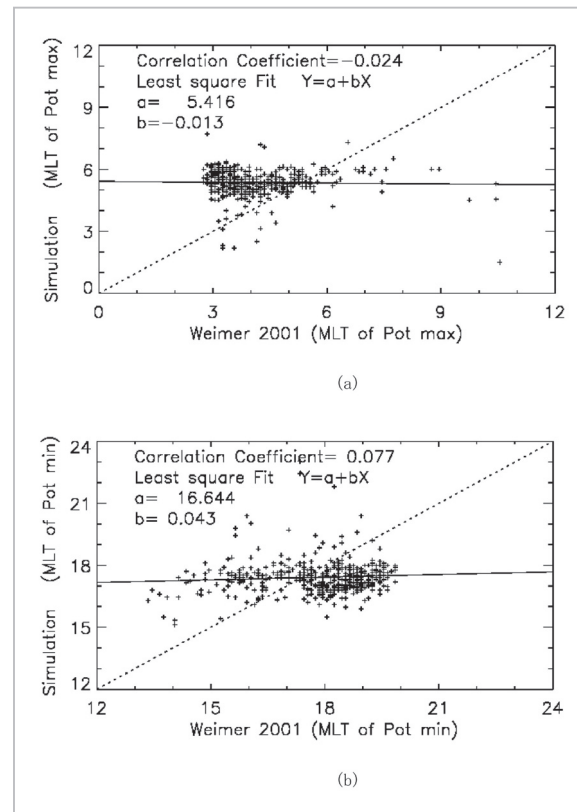


**Fig. 7** Comparative diagram between simulation and Weimer 2001 model regarding MLTs corresponding to the locations of maximal and minimal potential values

- (a) MLT corresponding to the location of maximal potential value
- (b) MLT corresponding to the location of minimal potential value

significant number of cases in the Weimer 2001 model as compared to the simulation.

## 5 Discussion on analysis results

### 5.1 Discussion on merging electric field ( $E_{merg}$ ) dependence of the CPCP value

The CPCP value resulting from simulation has a nearly linear relation with  $E_{merg}$ . The CPCP value resulting from the Weimer 2001 model also has a nearly linear relation with  $E_{merg}$ . The CPCP value obtained from simulation was found to be somewhat greater than that from the Weimer 2001 model in a comparison made of both values.

The following discusses the reasons why the CPCP value obtained from simulation is

somewhat larger, on the basis of understanding that such an empirical model as the Weimer 2001 model is not necessarily a perfect reference.

Ridley et al.[9] demonstrated that the CPCP value tended to become smaller under increased Pedersen conductance based on their study on the relation between both elements under the following conditions: ionospheric Hall conductance of 0 and uniform Pedersen conductance.

As the ionospheric Pedersen conductance is not uniformly distributed and Hall conductance is neither 0 nor uniformly distributed in our simulation, we should be careful about directly adopting such results. In our simulation, it is presumed that the ionospheric Pedersen conductance is generally set to a somewhat smaller value than the actual value. Verifying this presumption requires further study by setting a larger Pedersen conductance in our simulation and conducting a test.

The Weimer 2001 model may be used for data assimilation of our simulation in the future. Fujita[10] tried to conduct data assimilation where the variance between an AE index observed and that calculated from simulation was minimized by adjusting the conductance. By using a similar technique, data assimilation

could be considered where an effort is made to minimize the variance between the CPCP value of the Weimer 2001 model and that calculated from simulation by adjusting the conductance. During the process, studying how conductance changed from the value before data assimilation may provide clues to whether the presumption described above can be verified. Ideally, various types and aspects of verification should be conducted on data assimilation, then the results should be utilized for improving the simulation. Attention must also be paid to a specific point: when the simulation is tailored with one physical quantity for better consistency with the observation based on certain verification results, another physical quantity may conversely lose its consistency with the observation to a large extent. A comprehensive point of view is therefore required to realize a better simulation.

## 5.2 Discussion on IMF clock angle dependence of the magnitude relation between maximal value and minimal (absolute) values of potential

Table 1 summarizes the magnitude relation between the maximal and minimal (absolute) potential values. Statistical results from our

**Table 1** Clock angle (By polarity) dependence of magnitude relation between Potmax and |Potmin|

	90° < clock angle < 180° By > 0	180° < clock angle < 270° By < 0
NICT Simulation	Potmax <  Potmin	Potmax >  Potmin
Satellite observation statistical model (Weimer 2001)	Potmax <  Potmin	Potmax <  Potmin
Radar observation statistical model (Ruohoniemi and Greenwald 2005)	Potmax <  Potmin	Potmax <  Potmin

simulation indicate Potmax less than |Potmin| with positive By, and Potmax greater than |Potmin| with negative By. Conversely, Potmax is almost always less than |Potmin| regardless of positive/negative By in statistical results from the Weimer 2001 model when calculated using solar wind and IMF inputs under the same conditions as for simulation. According to the statistical results of SuperDARN radar observations reported by Ruohoniemi and Greenwald<sup>[11]</sup>, Potmax is less than |Potmin| regardless of positive/negative By. Ridley et al.<sup>[9]</sup> demonstrated that Potmax was less than |Potmin| in case of a steep gradient of Hall conductance from dayside to nightside. Our simulation demonstrated that Potmax is greater than |Potmin| with negative By.

Based on these results, we infer that the gradient of Hall conductance from dayside to nightside in our simulation is not so steep as the actual condition, but gradual. Our simulation used the following as forms of Hall conductance: (A) one due to solar EUV (solar extreme ultraviolet radiation), (B) one associated with pressure distribution of the magnetosphere, and (C) one associated with upward field aligned current<sup>[2]</sup>. The Hall conductance due to solar EUV is an element to produce the gradient from dayside to nightside. In contrast, intense (B) and (C) are elements to reduce the gradient of Hall conductance from dayside to nightside. Thus, we infer that (B) and (C) of Hall conductance in our simulation are set to values somewhat larger than the actual values.

### 5.3 Discussion on IMF clock angle dependence of MLTs corresponding to the locations of maximal and minimal potential

Our simulation results suggest that MLTs corresponding to the locations of both Potmax and Potmin are not systematically changed by the clock angle; the MLT for Potmax is located at about 5hMLT and that for Potmin at about 17hMLT. The reason why Potmax MLT and Potmin MLT are an hour earlier than 6hMLT and 18hMLT, respectively, is presumed to be the effect of the gradient of Hall conductance

from dayside to nightside being reflected to a certain extent in the simulation<sup>[12]</sup>.

According to a comparison of our simulation with the Weimer 2001 model, however, MLTs for both Potmax and Potmin obtained by the Weimer 2001 model are found located deeper into the nightside than those obtained by simulation. Ridley et al.<sup>[9]</sup> demonstrated that the potential distribution shifts toward the nightside when Pedersen conductance shows a steep gradient from dayside to nightside. Given this referenced finding, the gradient of Pedersen conductance from dayside to nightside is presumed in our simulation to be more gradual than in reality. In other words, by using the same logic as used in Section 5.2, we infer that items (B) and (C) of Pedersen conductance are set to values somewhat larger than in reality.

## 6 Summary

The MHD simulator running in real time for a long period of time using inputs from ACE observational data at the National Institute of Information and Communications Technology (NICT) was characterized through systematic studies on the simulator's dependence on solar wind, where enormous calculation results accumulated in a pseudo observational database were used for statistical analysis as if the calculation results were observational data. The parameters of focus were: CPCP value, maximal and minimal potential values, and MLTs corresponding to the locations of maximal and minimal potential (all extractable from the output two-dimensional distribution of the electric potential of the polar ionosphere). At the same time, we also conducted similar analyses on results provided by the Weimer 2001 model — an empirical model based on observations — with inputs selected from ACE observational data. This simulator was thus more clearly characterized based on a comparison of simulation results with results obtained from the Weimer 2001 model.

Based on a discussion of the analysis results, we infer that this simulation has the

---

following characteristics: (1) Pedersen conductance might be set somewhat smaller than in reality, and (2) the gradients from dayside to nightside for both Pedersen conductance and Hall conductance were slightly more gradual than in reality. The potential distribution resulting from this simulator is expected to be closer to reality in the future by improving the ways of providing conductance.

## Acknowledgments

We wish to thank the ACE MAG and SWEPAM instrument teams of the ACE Science Center for providing the ACE level 2 data. We also thank Dr. D. R. Weimer for the use of the Weimer 2001 model. Finally, we also wish to thank the Data Analysis Center for Geomagnetism and the Space Magnetism Graduate School of Science, Kyoto University for the use of provisional AL index data.

## References

- 1 Tanaka, T., "Generation Mechanisms for Magnetosphere-Ionosphere Current Systems Deduced from a Three-Dimensional MHD Simulation of the Solar Wind-Magnetosphere-Ionosphere Coupling Processes," *J. Geophys. Res.*, Vol. 100, pp. 12057–12074, 1995.
- 2 Tanaka, T., "The state transition model of the substorm onset," *J. Geophys. Res.*, Vol. 105, pp. 21081–21096, 2000.
- 3 Tanaka, T., "Formation of magnetospheric plasma population regimes coupled with the dynamo process in the convection system," *J. Geophys. Res.*, Vol. 108, 1315, doi: 10.1029/2002JA009668, 2003.
- 4 Den, M., T. Tanaka, S. Fujita, T. Obara, H. Shimazu, H. Amo, Y. Hayashi, E. Nakano, Y. Seo, K. Suehiro, H. Takahara, and T. Takei, "Real-time Earth magnetosphere simulator with three-dimensional magneto-hydrodynamic code," *Space Weather*, Vol. 4, S06004, doi: 10.1029/2004SW000100, 2006.
- 5 Weimer, D. R., "An improved model of ionospheric electric potentials including substorm perturbations and application to the Geospace Environment Modeling November 24, 1996, event," *J. Geophys. Res.*, Vol. 106, pp. 407–416, 2001.
- 6 Kitamura, K., H. Shimazu, S. Fujita, S. Watari, M. Kunitake, H. Shinagawa, and T. Tanaka, "Application of the Magnetospheric Model for Numerical Forecast – Validation Using the AE Index –," Special issue of this NICT Journal, 2-2-5, 2009.
- 7 Shimazu, H., K. Kitamura, T. Tanaka, S. Fujita, M. S. Nakamura, and T. Obara, "Real-time global MHD simulation of the solar wind interaction with the earth's magnetosphere," *Adv. Space Res.*, Vol. 42, pp. 1504–1509, 2008.
- 8 Boyle C., P. Reiff, and M. Hairston, "Empirical polar cap potentials," *J. Geophys. Res.*, Vol. 102, pp. 111–126, 1997.
- 9 Ridley A. J., T. I. Gombosi, and D. L. DeZeeuw, "Ionospheric control of the magnetosphere: conductance," *Ann. Geophys.*, Vol. 22, pp. 567–584, 2004.
- 10 Fujita, S., "The Global MHD Magnetosphere Simulation and Prospect for the Space Weather Prediction," Special issue of this NICT Journal, 2-3-4, 2009.
- 11 Ruohoniemi J. M. and R. A. Greenwald, "Dependencies of high-latitude plasma convection: Consideration of interplanetary magnetic field, seasonal, and universal time factors in statistical patterns," *J. Geophys. Res.*, Vol. 110, A09204, doi:10.1029/2004JA010815, 2005.
- 12 Tanaka, T., "Interplanetary magnetic field By and auroral conductance effects on high-latitude ionospheric convection patterns," *J. Geophys. Res.*, Vol. 106, pp. 24505–24516, 2001.



**KUNITAKE Manabu**

*Senior Researcher, Space Environment Group, Applied Electromagnetic Research Center*

*Magnetosphere Physics, Aeronomy*



**WATARI Shinichi, Dr. Sci.**

*Research Manager, Space Environment Group, Applied Electromagnetic Research Center*

*Solar-Terrestrial Physics, Space Weather*



**SHINAGAWA Hiroyuki, Ph.D.**

*Senior Researcher, Space Environment Group, Applied Electromagnetic Research Center*

*Ionospheric Physics*



**SHIMAZU Hironori, Dr. Sci.**

*Senior Researcher, Space Environment Group, Applied Electromagnetic Research Center*

*Space physics*



**NAGATSUMA Tsutomu, Dr. Sci.**

*Research Manager, Space Environment Group, Applied Electromagnetic Research Center*

*Solar-Terrestrial Physics*



**HORI Tomoaki, Dr. Sci.**

*Assistant Professor, The Solar-Terrestrial Environment Laboratory, Nagoya University*

*Magnetosphere Physics*



**FUJITA Shigeru, Dr. Sci.**

*Associate Professor, Meteorological College*

*Physics of the magnetosphere-ionosphere system*



**TANAKA Takashi, Dr. Sci.**

*Professor, Graduated School of Sciences, Kyushu University*

*Magnetospheric Compound System Physics*